Construction and Building Materials 408 (2023) 133765

Contents lists available at ScienceDirect

Construction and Building Materials

journal homepage: www.elsevier.com/locate/conbuildmat

Development of a nature-inspired polymeric fiber (BioFiber) for advanced delivery of self-healing agents into concrete

Mohammad Houshmand Khaneghahi [a,*], Divya Kamireddi [b], Seyed Ali Rahmaninezhad [a], Amirreza Sadighi [c], Caroline L. Schauer [b], Christopher M. Sales [a], Ahmad R. Najafi [c], Aidan Cotton [a], Reva Street [b], Yaghoob (Amir) Farnam [a]

[a] Department of Civil, Architectural and Environmental Engineering, Drexel University, Philadelphia, PA, US
[b] Department of Materials Science and Engineering, Drexel University, Philadelphia, PA, US
[c] Department of Mechanical Engineering and Mechanics, Drexel University, Philadelphia, PA, US

ARTICLE INFO

Keywords:
Calcium carbonate
Endospore
Hydrogel
Self-healing
Polymeric Fiber

ABSTRACT

In this study, we developed nature-inspired multi-functional polymeric fibers (called BioFiber) to deliver bio-self-healing agents into cementitious materials. BioFibers were manufactured using a load-bearing core-fiber, a sheath of endospore-laden hydrogel, and an outer damage-responsive polymeric shell layer. The innovative BioFiber integrates three key functionalities into the quasi-brittle matrix: (i) autonomous bio-self-healing, (ii) crack growth control, and (iii) damage-responsiveness. The hydrogel sheath contained endospores, as bio-agents, to establish microbially-induced calcium carbonate precipitation (MICCP) as a self-healing end-product. The core-fibers provided crack growth control functionality into quasi-brittle engineering materials. Additionally, the outer shell coating integrated a robust damage-responsive self-healing activation strategy in concrete. A comprehensive parametric study was conducted to explore material options and the influential parameters for tailoring the processing-compositions-structure properties of the developed BioFiber. The findings of this study revealed that a concentration of 8 w/v sodium-alginate crosslinked with calcium acetate provided higher solution uptake capacity required for MICCP. As for the shell, the polymer blend of polystyrene and polylactic acid (1:1 wt%), with polymer/solvent ratio of 18 w/v-single layer coating, effectively protected BioFibers during simulated concrete casting process. Lastly, each BioFiber was able to produce 40–80 mg of calcium carbonate within the first 30 h of activation.

1. Introduction

Self-healing is the intrinsic capability of a material to repair a physical degradation without external intervention and either partially or fully recover its pre-damage state [1–4]. Natural organisms demonstrate the ability to self-heal when non-catastrophic damages occur due to intrinsic complications or/and extrinsic menaces [5–8]. The self-healing functionality in living organisms grants extended longevity and adaptation to environmental changes [9,10]. Wound healing, for instance, is one of the common self-healing processes in biological systems. The performance of engineering materials, such as cementitious composites, is dominated by irreversible chemical/physical degradation processes which leads to thermodynamic, chemical, and mechanical instability of materials [11–14]. The degradation mechanism involves a combination of internal and external factors, including alterations in microstructure and composition, deformation over time, exposure to corrosive substances, and challenging environmental conditions [15]. The execution of strategies aimed at preventing or mitigating degradation can incur significant costs, consume considerable time, and pose practical challenges [16]. Self-healing capability provides shelf-life extension and enhanced mechanical integrity to engineering materials. Researchers have shown growing interest in nature-inspired self-healing functionality to integrate self-healing properties into engineering materials [17,18], which can prolong the service-life of materials, reduce the materials inefficiency, and have desirable economic attributes [19]. Moreover, self-healing materials are suggested to provide sustained performance reliability, especially in areas with limited accessibility [20]. Considering that different living organisms have distinctive

* Corresponding author.
E-mail address: mhk58@drexel.edu (M. Houshmand Khaneghahi).

https://doi.org/10.1016/j.conbuildmat.2023.133765
Received 24 July 2023; Received in revised form 5 October 2023; Accepted 9 October 2023
Available online 17 October 2023

healing mechanisms [21] it is hypothesized that the healing process and its delivery strategy need to be tailored for each engineering material [20]. In the realm of self-healing materials, a biomimetic engineered materials are those featuring self-healing features mainly through systematic transport of self-healing agents [22]. Self-healing mechanisms have been integrated into various materials such as metals, alloys, ceramics, polymers, and composites [23].

An innovative autonomous self-healing mechanism used in quasi-brittle engineering materials, such as cementitious composites, is to utilize bacterial-induced calcium carbonate precipitation (MICCP) process [24]. This technique is performed through the reaction of carbonate, a common metabolic end-product of many microorganisms, with calcium ions to form calcium carbonate. The harsh conditions in concrete, e.g., high pressure, temperature, alkaline condition, and unavailability of sufficient oxygen, can adversely affect microbial activity and survivability [25–27]. Since endospores of bacteria, metabolically inactive form of vegetative cells, can remain dormant for prolonged periods with high survivability rate in extreme conditions, this bacterial phenotype is often favored for MICCP [28]. In the presence of carbon and nutrient sources, endospores can be induced to from its dormant state (endospores) to become vegetative cells in a process initiated by germination [29]. In addition to using endospores, several delivery methods such as encapsulation and creation of vascular network, have been applied to protect bio-agents to deliver and integrate autonomous self-healing functionality into cementitious matrices [30–36].

The encapsulation of self-healing agents in different carries have been proposed by previous studies to protect bacteria and self-healing agents in quasi-brittle cementitious composites from extreme environments and harsh manufacturing processes [30–32,37–40]. When cracks form in quasi-brittle materials, the carrier ruptures along the crack path, leading to the release of healing agents into the crack due to capillary pressure and gravitational forces [41]. Either organic or inorganic materials can be used to synthesize healing agent's carrier capsule [42], including polyurethane, polyurethane, ethylene cellulose, poly styrene–divinylbenzene, urea–formaldehyde, phenol–formaldehyde resin, bio-hydrogel, alginate, colloidal silica, silica gel, sodium silicate, melamine formaldehyde, bentonite nano/micro particles, graphite nanoplate [43–46]. Wang et al. investigated using hydrogel capsule as bio-healing agents [47]. They utilized tri-block copolymer of poly (ethylene oxide) and poly (propylene oxide) as a swollen hydrogel. They prepared the bacterial reagent suspension using Bacillus Sphaericus, yeast extract (20 g/L), and urea (20 g/L). In addition, they prepared polymer solution (20 % wt.) and added 8 g/L of photo-initiator to the solution. The UV radiation was applied to the mixture of bacterial and polymer solutions to crosslink the polymers via free radical polymerization technique. After crosslinking stage, they freeze-dried the products and grind them to produce capsules with the size of 5 to 20 μm. Their results indicated that the maximum healed crack width was about 0.5 mm, with a 68 % reduction in water permeability.

One of the major challenges in autonomous encapsulation method is to control self-activation of healing agents (i.e., damage-responsiveness or induction of MICCP activity of the spores) to coincide with crack occurrences [48]. To address this issue, several studies have investigated the development of shell/core capsules that have a brittle strain-responsive shell material that breaks upon cracking [31,49–51]. Jiang et al. manufactured a composite shell structure using melamine phenolic resin with modified sodium alginate [46]. The particle size, thermal stability, and coating ratio of micro-capsules were tuned by sodium alginate properties such as adhesion and degradability [46]. Melamine phenolic resin provided brittleness and hardness to the capsule shell. For the capsule core, two-component epoxy resin was used as healing agent [46]. Manufacturing of shell/core capsules was performed at three stages: (i) pre-polymerization, (ii) emulsification, and (iii) curing. In the first stage, the melamine phenolic was fed to the solution with pH of 8–9 with the temperature of 70 °C. Sodium alginate, emulsifier, and epoxy resin was added to the solution, uniformly stirred at 600 rpm, to form an oil/water solution. In the final stage, the solution was filtered to obtain the capsules, then placed in 50C vacuum drying for 24 h. The final size of cured microcapsule was about 55 μm and the core-to-shell coating ratio of 65 %. They determined the microcapsule optimum content in the concrete, i.e., 4 %, leading to efficient self-healing ability for micro-cracks. Despite the significant advantages of autonomous encapsulation technologies, these techniques have not been widely mass-produced due to their complicated preparation process, resulting in an uneven distribution, lower mechanical properties, and expensive manufacturing process/material [52,53].

Several researchers also investigated the feasibility of embedding damage-responsive brittle hollow tubes, or creating vascular network in composite materials, to incorporate chemical/bacterial healing agents into them [54–56]. These tubes and vascular network provide large void volumes to incorporate higher amounts of healing agents. In addition, the vascular network creation can be controlled in the manufacturing process, preventing the dispersion randomness of the spherical capsules [55]. A novel approach to create vascular network in the cementitious composite is using 3D printing approach [35,36,57]. The three-dimensional vascular structures can be created with any complex geometry based on the target application. In terms of autonomous vascular self-healing, brittle/removeable materials are used to facilitate initiation of self-healing mechanism. The 3D channel network provides transportation of healing agents into the cementitious matrix. Furthermore, several studies have investigated the influence of vascular network on mechanical/fracture properties of the concrete as well as the self-healing efficiency. Using incompatible materials, e.g., silicone, polyvinyl chloride, and polyethylene terephthalate, which possess different elastic modulus with concrete may cause delamination, resulting in lower autonomous healing efficiency [35,36]. In a study done by Wan et al., they designed an octet-structure lattice made of acrylonitrile butadiene styrene (ABS) for creating the vascular network to deliver the healing agent to the crack regions [35].

Although imitating self-healing in materials has introduced an era of novel smart materials, the field is in the infancy. Designing self-healing processes in materials by well-established synthetic paths is challenging [58]. The advantages and disadvantages of existing self-healing delivery methods for concrete application can be summarized through the following criteria: (i) abundance of healing agents, (ii) stability of healing agents, (iii) damage-induced activation, (iv) impact on matrix defects, (v) control of crack growth, (vi) feasibility of implementation, and (vii) complexity in manufacturing. In the case of direct incorporation, self-activation and self-termination are absent, as the healing agents can initiate the healing process upon exposure to the matrix. Moreover, it has been observed that directly dispersed agents can effectively heal cracks with small openings. Regarding encapsulation, the survivability of healing agent and damage-responsiveness has been provided using core/shell capsule. However, the primary challenge in encapsulation lies in controlling crack propagation, especially when dealing with the intricate manufacturing process associated with shell/core capsules. When it comes to vascularization, abundant of self-healing agent can be provided to the cracked area and activation can be initiated by localized damage. Nonetheless, the creation and implementation of a complex vascular network within concrete can prove to be a challenging endeavor.

Based on the given discussion, there are various aspects of self-healing that are not thoroughly covered in the current state of the literature. One of the highly important aspects is to incorporate self-healing robustness in terms of featuring damage-responsiveness and controlled crack propagation. A major challenge in autonomous self-healing is to control crack growth while healing takes place, similar to skin biological tissues in nature. Furthermore, the existing literature lacks extensive understanding regarding the enhancement of the survival and long-term effectiveness of bio-inspired or bio-based healing agents. Hence, investigating the feasibility of developing a bacterial-based self-healing system with controlled crack growth and damage-

responsive capabilities is of paramount significance. In this paper, we share the development of a novel delivery/activation system to establish a robust autonomic self-healing paradigm by developing multi-functional microbial-based fibers (called BioFiber hereafter) for bio-self-healing agent delivery in quasi-brittle cementitious composites. The proposed Bio-Fiber self-healing strategy in quasi-brittle cementitious composites is schematically illustrated in Fig. 1. In the first stage, damage initiation, crack opens on the surface of cementitious matrix allowing water and oxygen penetrates through micro-crack from surrounding environment. In the second stage, cracks propagate, breaking damage-responsive impermeable fiber shell layer, exposing the endospore-laden hydrogel to water and oxygen. The hydrogel swells and disperses the endospore into the crack volume, exposing them to water, oxygen, and nutrients within crack volume. In the third stage, the germinated endospore produces self-healing end-products, i.e., Microbial Induced Calcium Carbonate Precipitation (MICCP), healing the exposed cracks.

The novelty of BioFiber is to engineer key functionalities in BioFiber that can be integrated into the quasi-brittle matrix to enable not only self-healing, but also enhance mechanical response. The key functionalities include: (i) autonomous bio-self-healing, (ii) crack growth control, and (iii) damage-responsiveness. To achieve this functionalities, various technical challenges are addressed in this study including:

- Incorporation of desirable biological self-healing organisms in BioFiber that can survive in concrete harsh fresh and hardened conditions until the moment it is needed to heal the quasi-brittle materials;
- Finding desirable polymer material that can provide sufficient bridging in the quasi-brittle materials during crack formation to control crack growth; and
- Designing a polymer material that not only protects the biological organisms from concrete harsh environment, but also possesses desirable mechanical strain-responsiveness to activate the BioFiber when crack occurs.

To engineer the three key functionalities and address the aforementioned challenges, BioFiber will be manufactured using three different layers: (i) polymeric core-fiber as load-bearing/energy-absorber element, (ii) sheath of endospore-laden alginate hydrogel, and (iii) damage-responsive polymeric outer shell layer. The core-fibers provided crack growth control functionality into cementitious composites. The hydrogel sheath contained endospores, as bio-agents, to establish MICCP as a self-healing end-product. The outer polymeric shell coating integrated a robust damage-responsive self-healing activation strategy in the matrix. The main challenge in BioFiber development is to explore material options and the influential parameters for tailoring the processing-compositions-structure properties of the developed BioFiber.

2. Materials and methods

2.1. Materials

Various material options have been investigated in this study to tailor the processing-compositions-structure properties of the developed BioFibers to achieve multifunctionalities. The detailed descriptions of the materials properties are discussed in the following.

2.1.1. Polymeric Core-Fiber

Inner polymeric core-fiber has been used as the first element in BioFiber to deliver desirable mechanical properties. Since the primary functionality of the core-fiber is to integrate load-bearing and energy absorption to the BioFiber, it also requires providing a proper environment for proliferation of endospores infused within the hydrogel sheath. In this study, polyester (PES) and polyvinyl alcohol (PVA) fibers have been selected as core-fibers, providing robust mechanical properties and bio-compatibility characteristics. PVA fibers used in this study were commercial water-insoluble fibers (NYCON RF4000) produced mainly for concrete applications. PES fibers were purchased from Unifi, as recycled polyester. The material/geometrical properties of the core-fibers used in this study are listed in Table 1, reported by manufacturer.

2.1.2. Endospore-laden hydrogel

In the current study, Lysinibacillus sphaericus strain MB284 was used as a bio-healing agents to be loaded in hydrogel sheath. Germination of endospore was triggered by the presence of carbon and nutrient source, i.e., yeast extract and urea, and urea hydrolysis-driven MICCP was initiated by the presence of calcium source. Yeast extract was purchased from Sigma-Aldrich (CAS:8013–01-2), urea from Alfa Aesar (CAS:57-13-6). Our previous studies have revealed that the thermal shock endosporulation method resulted in production of endospores that can survive, germinate, and grow under inhospitable conditions

Table 1
Polymeric core-fiber material/geometrical properties.

Properties	Polyester (PES)	Polyvinyl alcohol (PVA)
Length (mm)	Varied	30
Diameter, Average (μm)	301	611
Diameter, Standard Deviation (μm)	20	19
Density (g/cm^3)	0.63	1.44
Tensile Strength (MPa)	181	800
Elastic Modulus (GPa)	0.8	23
Morphology	Multi-Filament	Mono-Filament

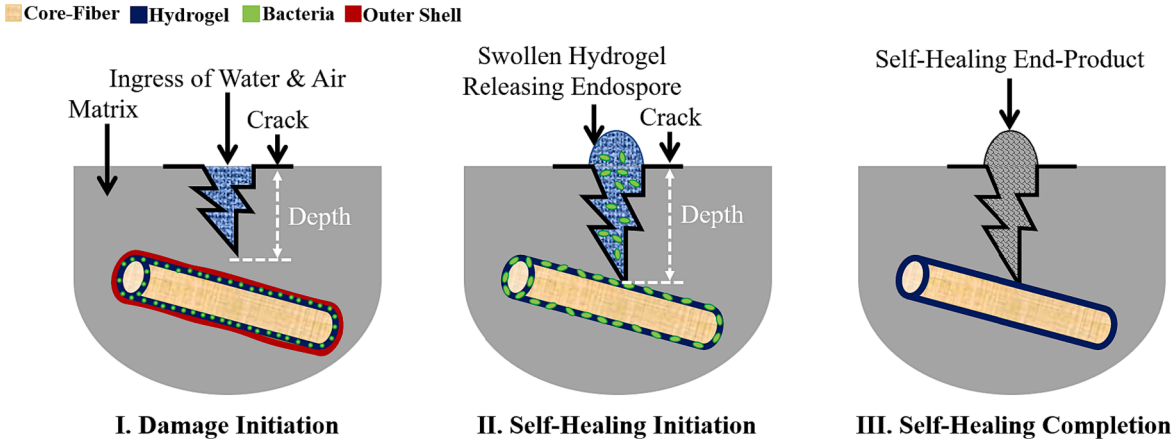

Fig. 1. Schematic illustration of BioFiber self-healing stages in quasi-brittle cementitious composite shown in grey color.

Table 2
Polymeric material options for BioFiber shell coating.

	Shell Material	Solvent/Initiator	Curing/Polymerization Condition
1	Nitrocellulose (NITR)	–	1 h, RT*
2	Epoxy Resin (ER)	Aliphatic Polyamine Hardener	24 h, RT
3	Polymethylmethacrylate (PMMA)	Benzoin Benxzoyl peroxide	2 h Ultraviolet radiation (wavelength: 340 nm, irradiance: 0.89 W/(m^2.nm)
4	Polyvinylidene Fluoride (PVDF)	Dimethoxypropane (DMP)	1 h, RT
5	Cyanoacrylate Adhesive (CYA)	–	½ hour, RT
6	Polystyrene (PS)	Chloroform	½ hour, RT
7	Polylactic Acid (PLA)	Chloroform	½ hour, RT *RT: Room Temperature (23 ± 1 °C)

[28]. In the thermal shock method, Lysinibacillus sphaericus vegetative cells were firstly incubated into the culture medium, i.e., yeast extract (20 g/L) and urea (20 g/L), for 24 h to reach the exponential growth phase of the cells. Then, the vegetative cells were washed three times with 1 M of Phosphate Buffer Solution (PBS) and inoculated into the Minimal Salt Media (MSM) [28]. In the next stage, the cells were incubated for 30 min in a boiling water bath followed by 30 min in an ice water bath (referred to as the thermal shock endosporulation method). Our previous studies have shown that the endospores produced through thermal shock method can germinate in harsh alkaline condition (pH of 12), high salinity environment (up to 100 g/L), and under freeze–thaw cycles (temperature of −10 to 60 °C) [28]. The germination rate of Lysinibacillus sphaericus strain MB284 endospores are 1.42 OD_{600} per day [28]. The survival rate of the endospores have been found to be 82 % under saline condition (50 g/L of NaCl), 94 % under freeze–thaw cycles (−4 °C and 25 °C for 7 days) and %100 for pH of 12 [59]. The germination lag phase for the endospores was measured to be 8 h [28,59,60]. For hydrogel, sodium-alginate (Na-Alg) and calcium chloride and calcium acetate, as a source of divalent cations, have been used. The concentration of Na-Alg solution was selected based on previous studies in the range of 2–8 w/v. Previous researchers have selected a sodium alginate concentration in a range of 1–4 w/v to create alginate-based capsules and beads [32,61–63]. In this study, in which is hydrogel coating on core-fiber rather than beads creation, the values were increased up to 8 w/v to investigate the effects of higher sodium alginate viscosity on the amount of hydrogel that can be loaded on the core-fiber. Sodium-alginate was purchased from Sigma-Aldrich (CAS: 9005-38-3), calcium chloride dihydrate from MP Biomedical (CAS: 10035-04-8), and calcium acetate monohydrate from CHEM-IMPEX INT'L INC (CAS: 5743-26-0).

2.1.3. Polymeric outer shell layer

To integrate damage-induced healing mechanism into the BioFiber, a strain-responsive polymeric-based shell coating was proposed as the outer layer on the hydrogel coated core-fiber. Assorted polymeric materials have been shortlisted, as shown in Table 2, to further be experimentally investigated to meet the mentioned shell coating requirements.

2.2. BioFiber manufacturing

A surface functionalization method defined as instant immersion has been used to manufacture the BioFibers. This technique included the soaking of the core-fibers (PES and PVA) in three solution baths such as: (i) Na-Alg/endospore solution, (ii) calcium crosslinker solution, (iii) polymeric-based coating solution or uncured/pre-crosslinked liquid. For the first step, which is loading endospore-laden hydrogel on the core-fiber, Na-Alg powder mixed with endospore suspension with a concentration of 10^9 cell/mL, and gently stirred for 1 h. In general, a high bacterial concentration can begin to interfere with gel formation when the polymer chains encounter challenges in accessing calcium ions [64]. In this study, we utilized a typical concentration for endospore, i.e., 10^9 cells/mL, to be incorporated in hydrogel. Calcium chloride and calcium acetate solutions have been prepared in deionized water. The core-fibers, with the length of 30 mm, were first soaked in the Na-Alg/endospore solution, then, they were soaked in calcium crosslinker solution to trigger ionic crosslinking process. In both stages, the immersion in the solution was immediate, with no delay in the soaking process. After a sheath of endospore-laden hydrogel was created on the core-fibers, the fibers were set to dry under ambient condition (23 °C) for 24 h. In order to tune the coating thickness and swelling capacity of the hydrogel, the concentration of the alginate solution was changed as 2, 4, 8 wt-to-volume (w/v). In this study, the concentration of calcium crosslinker solution kept constant at 0.259 M.

In the next step, which is applying impermeable strain-responsive polymeric shell coating on the BioFibers, different polymeric solutions were prepared based on the type of the shell materials. In the case of lacquers polymers (e.g., Nitrocellulose), the shell coating process was governed by evaporating solvents used in formulation of lacquers. Shell bath contains the polymer/solvent solution. For reactive prepolymers and polymers, e.g., epoxy resin, the shell bath contained the prepolymers mixed with co-reactants, of which the polymerization occurred through an exothermic reaction between reactive and co-reactants materials. For Methyl methacrylate (MMA) polymerization, free radical polymerization (FRP) technique was used to create a shell layer on the BioFibers. In this method, benzoyl peroxide and benzoin (each 0.5 g in 10 mL of MMA) were used as a photo-initiator, decomposed into free radicals under irradiation of ultraviolet (UV) light, synthesizing Polymethylmethacrylate (PMMA) film on the BioFiber. Benzoyl peroxide under UV irradiation resulted in formation of two benzoyloxy radicals and benzoin generated benzoyl and α-hydroxybenzyl radicals as an initiation stage for the FRP mechanism. In the next stage (i.e., propagation), the free radicals attached the MMA monomer, building polymer chains. The polymer chain length and the termination stage of FRP depends on the photo-initiator concentrations. Since the different polymerization methods with various polymeric materials were used, the different drying/curing/polymerization conditions were applied, as shown in Table 2.

Table 3
Experimental program for BioFiber performance assessment.

Experiment	Objective
Optical Microscopy	To visually investigate the hydrogel and outer shell coating morphology on the core-fibers
Scanning Electron Microscopy	To perform microstructural analysis on the BioFiber after each surface coating applied on the core-fiber
Gravimetric Swelling Analysis	To determine the swelling capacity of endospore-laden hydrogel in different conditions
Fluid Ingress Survivability Test	To investigate the impermeability of outer shell coating against ingress of aqueous solution
Abrasion Resistance	To study the abrasion resistance of the shell coating under simulated casting process
Thermogravimetric Analysis	To quantify the amount of precipitated calcium carbonate via MICCP activity

2.3. Experimental program

To evaluate the performance of the manufactured BioFiber, an experimental program was developed based on the functionality of hydrogel, shell coating, and the overall BioFiber, as shown in Table 3. Detailed experimental programs are discussed in the following sections.

2.3.1. Coating morphology assessment

The thickness and uniformity of coating are important since these factors can influence the overall functionality and cost of the BioFiber. In this study, optical microscopy was used to determine the thickness and uniformity of the endospore-laden hydrogel coating loaded on the polymeric core-fiber. The hydrogel thickness to core-fiber diameter ratio was calculated based on the thickness measurement as:

$$t_{Hgel\%} = (t_{Hgel}/D_{cf}) \times 100 \quad (1)$$

where $t_{Hgel\%}$ is the hydrogel thickness ratio in percentage, t_{Hgel} is the hydrogel thickness, and D_{cf} is the core-fiber diameter. In addition, the weight of hydrogel loaded on the core-fibers was calculated using the following equation:

$$W_{Hgel}(mg/mg/cm) = (W_{FH} - W_F/W_F)/L_F \quad (2)$$

where W_{Hgel} is the normalized weight of hydrogel loaded on the core-fiber to the length of the fiber (mg/mg/cm), W_F is the initial weight of core-fibers, W_{FH} is the weight of hydrogel coated core-fibers, and L_F is the length of the core-fiber. To ensure repeatability of measurements, 30 samples were used for this test, with 10 measurements over the length of each fiber. For the hydrogel coating morphology study, the hydrogel was prepared using 2, 4, 8 w/v of Na-Alg crosslinked with calcium acetate (CA) and calcium chloride (CC) with constant concentration of 0.259 M.

Similar to hydrogel coating, the morphology assessment of shell coating finish on the BioFibers is important to ensure manufacturing of a high-performance BioFibers. The shell coating morphology on the BioFibers governs the interfacial properties between the concrete and the fibers, crack-bridging functionality, and the protection of inner layers. To perform morphology assessment, an optical microscopy technique was utilized to determine the shell coating uniformity and the thickness ratio. In this experiment, the hydrogel was prepared using 8 w/v of Na-Alg, crosslinked using calcium acetate with molarity of 0.259. For measuring the coating thickness for each shell material, five replicate samples were prepared with 10 measurements reading on each sample. The shell coating thickness to hydrogel coated core-fiber was calculated based on the thickness measurement as:

$$t_{Shell\%} = (t_{Shell}/D_{hcf}) \times 100 \quad (3)$$

where $t_{Shell\%}$ is the shell coating thickness ratio in percentage, t_{Shell} is the shell coating thickness, and D_{hcf} is the diameter of the core-fiber with hydrogel coating core-fiber.

2.3.2. Microstructural analysis

To perform microstructural analysis on the BioFiber after manufacturing process, before/after MICCP activation. Samples were coated with a 12 nm thick layer of 80/20 platinum/palladium using a Cressington 208 sputter coater (Ted Pella, Inc., Redding, CA), since the materials used for BioFiber manufacturing are nonconductive. Scanning electron microscopy (SEM) was then performed using a Zeiss Supra 50/VP to observe fiber morphology on all samples.

2.3.3. Endospore-Laden hydrogel swelling performance

Swelling capacity is one of the most technical features of hydrogels, impacting the MICCP urea hydrolysis-driven chemical pathways through controlling the amount of water delivered to the endospores. The swelling ratio is defined as the quantity of the mass gain of the hydrogels as exposed to aqueous solutions at various time intervals. To determine the swelling ratio, gravimetric analysis was performed on the endospore-laden hydrogel coated core-fibers at dry and wet state. First, dry pre-weighted endospore-laden hydrogel coated core-fiber samples were immersed in excess of swelling medium. After certain exposure time intervals, the samples were removed from the swelling medium, with excess solution being cleared away from each sample surface by wiping with a soft tissue cloth, and then weighed immediately. The swelling ratio based on these weights were calculated according to the following equation:

$$S_r = (W_s - W_d)/W_d \quad (4)$$

where S_r is the swelling ration, W_s and W_d are the weight of the samples in swollen and dry state, respectively. Since the swelling capacity is highly affected by the hydrogel structures, a parametric study was performed on the effects of the Na-Alg concertation, i.e., 2, 4, 8 w/v, and the cation crosslinker type, CA and CC, on the swelling ration. In addition, the pH of aqueous solutions has been changed as 3, 5, 7, 10, and 13 to study the swelling ratio sensitivity to acidic, neutral, and basic conditions. The swelling ratio was calculated at consecutive time intervals of 2, 5, 10, and 15 min. For each set of tests, five replicates were used to ensure the measurement repeatability.

2.3.4. Fluid ingress survivability test

Impermeability test was performed to investigate whether the shell coating can protect the endospore-laden hydrogel from unwanted access to moisture and/or aqueous solution. The impermeability test was designed based on monitoring the pH-sensitive indicator color change as BioFibers with different shell coating materials exposed to aqueous medium. Phenolphthalein, an organic-based acid-base indicator, was blended with the Na-Alg/endospore solutions with the concentration of 0.1 w/v, and hydrogel and shell coating on the core-fibers was performed with the similar steps, as discussed earlier. Phenolphthalein is colorless at pH below 8.5, reaching pink to deep purple color at medium with pH above 9. Using this feature, the BioFibers were exposed to high alkaline synthesized pore solution for time intervals of 1 and 2 h(s). In the case of permeable shell coating, the solution reached the inner layers, exposing phenolphthalein to high pH and color change. Observing pink/purple color on the surface of the BioFibers was considered as an indication of permeable shell coating. In the case of impermeable shell coating, no color change was observed on the surface or in the exposed solutions. The color change observation was performed using an optical microscope.

2.3.5. Abrasion resistance performance

Since the primary purpose of developing BioFibers is to incorporate into a quasi-brittle matrix to enable self-healing, the survivability of shell coating during blending manufacturing, i.e., using shear mixers which applies shear loading stresses to the BioFibers. is one of the important factors that needed to be investigated. In the BioFibers manufacturing, similar to fluid ingress survivability test, 0.1 w/v of phenolphthalein was blended with hydrogel. The shell materials used for this experiment were those materials shortlisted based on the impermeability test results. Using a typical fiber reinforced cementitious mortar sample mixture (as shown in Table 4), the BioFibers were incorporated into the mixture without binder materials. In the context of

Table 4
Mortar mix design for simulated casting process.

Material	Volume (%)	
	Typical	Used in This Study
Cement	25.31	0.00
Water	33.69	33.69
Standard Sand	40.00	65.31
Fiber	1.00	1.00
Total	100.00	100.00

this study, the process of mixing BioFiber with standard sand and a solution was conducted without the inclusion of cement. This approach was adopted to facilitate subsequent casting survivability tests. The presence of a binder would have impeded the ability to effectively separate BioFibers following the simulated casting process and calculate the BioFiber survivability rate. The amount of binder excluded from the concrete mix replaced with the standard sand, to introduce more severe casting condition. For each set of tests, 20 number of BioFibers were used, mixed with the standard sand and water using two methods: manual hand mixing and mechanical mixing using a shear mixer. After mixing stage, the samples were separated from the other component to observe whether they remained intact or fractured. The separation phase during the casting survivability test was conducted in a two-step process. Initially, the sand was separated using a sieve, with any residual BioFibers collected on top of the sieve. Subsequently, to confirm that no BioFibers had passed through the sieve, the sand was transferred to a large tray, and any remaining BioFibers were diligently collected until the total count of BioFibers before and after the casting process aligned. The survivability (%) was defined based on the number of intact BioFibers over the total number of BioFibers used. The BioFiber mixing process with mortar components were performed with two methods: (a) 2-minute manual mixing (MM), and (b) 2-minute mechanical shear mixing (MSM) using a vacuum shear mixer with 350 rps. The hand mixing and mechanical mixing were used to study the impact of using different mixing methods on the casting survivability of the BioFibers. After the mixing stage, the samples were poured on a tray, and the BioFibers were separated from water and sand. Then, the BioFibers were exposed to alkaline synthesized pore solution with pH of 13 for 1 and 2 h. Finally, the BioFibers were examined under an optical microscope to detect color change on the surface of the BioFibers. Since the impermeable shell materials were used for this experiment, any color change or release was associated with the shell fracture during the casting process.

2.3.6. MICCP performance

Previous experiments were designed to evaluate the performance of BioFiber elements, i.e., hydrogel and shell. In this stage, the objective was to conduct a quantitative/qualitative analysis of calcium carbonate precipitation as an end-product of urea hydrolysis-driven chemical reactions to heal quasi-brittle materials. In order to promote self-healing process, the fractured and intact (as control sample) BioFibers are exposed to a solution media containing yeast extract, urea, and calcium acetate (each with a concentration of 20 g/L) for 30 h. No MICCP activity was hypothetically expected in the case of intact BioFibers. In fractured BioFibers, the hydrogel absorbs water, releasing endospores to the media. Then, endospores sensed the organic carbon source, i.e., nutrients, allowing them to initiate germination and outgrowth stages. The calcium acetate provided the calcium ions for the final precipitation of calcium carbonate. To quantify the amount of precipitated calcium carbonate, thermogravimetric analysis (TGA) was performed on the solid residue after MICCP termination. After exposing the BioFibers to a calcium/carbon source, the solution media was centrifuged for 9 min at 7830 rpm and a temperature of 25 °C to terminate the MICCP process and further obtain the residue. The residue was kept at 105 °C for 1 h to remove the remaining water/moisture from the samples. Then, the solid residue was grinded to collect the particles with sizes less than 75 μm. An amount of 20–30 mg of the samples were deposited at a high-temperature platinum pan, and TGA tests were conducted at 30–900 °C with a ramp rate of 10 °C/min.

3. Results and discussions

3.1. Hydrogel Physical/Morphological properties

The hydrogel layer thickness was adjusted by changing the concentration of prepolymers, i.e., Na-Alg. The thickness measurements were performed using an optical microscope, and the results are shown in Fig. 2. For both PES and PVA core-fiber, an increasing trend on the hydrogel thickness was observed as the concentration of Na-Alg increased. This trend was associated with the increase in prepolymer viscosity as the prepolymer concentration increased. Higher prepolymer concentration increased hindrance and friction among the polymer chains, increased the prepolymer solution viscosity, and resulted in higher adherence of Na-Alg into the core-fibers. For instance, the hydrogel crosslinked with calcium acetate on the PES led to hydrogel thickness of 4.65 % and 16.61 % for Na-Alg concentrations of 2 and 8 w/v, respectively. From a gelation time perspective, the increase in prepolymer concentration leads to slower rearrangement of the polymer chain conformations. However, since the crosslinking reaction was completed in a single instant soaking step in a crosslinker bath, the gelation time was not a key factor affecting BioFiber manufacturing. Although the concentration of cation crosslinker solutions was constant at 0.259 M of Ca^{2+}, the hydrogel coating formation on the core-fiber was slightly thicker in all cases as calcium acetate solution was used compared with calcium chloride. The observed disparity in crosslinker cations, i.e., calcium chloride and calcium acetate within our

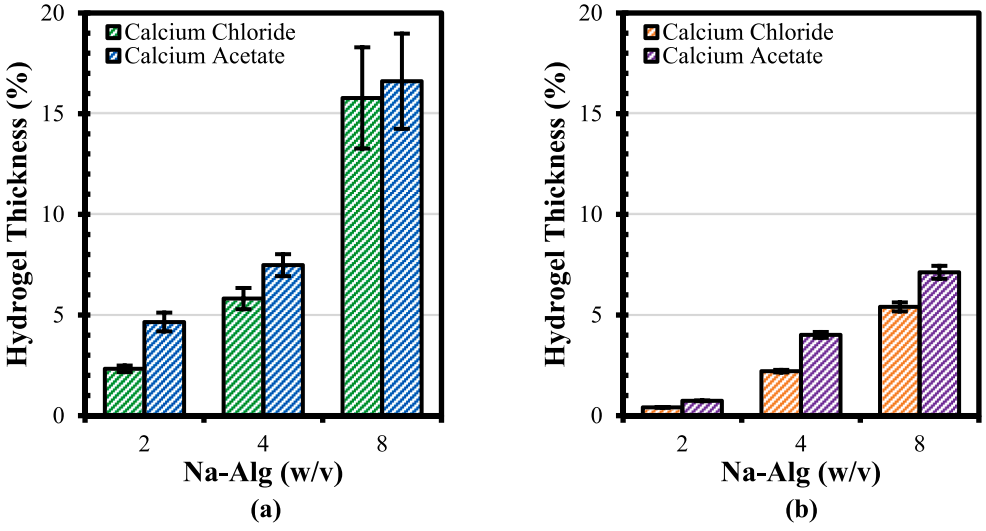

Fig. 2. Hydrogel coating thickness, as calculated using Eq. (1), versus sodium-alginate solution: (a) PES, (b) PVA (the statistic shown this plot is based on 30 replicates for each set of samples).

investigation, is potentially attributed to variations in ionic strength [65,66]. While both calcium chloride and calcium acetate furnish an equivalent number of calcium ions per molecule (as the molarity remains consistent in both solutions), the ionic strength of the solution may diverge. Calcium chloride contributes chloride ions (Cl^-) upon dissolution, whereas calcium acetate in aqueous medium releases acetate ions (CH_3COO^-). It is plausible that calcium ions exhibit distinct affinities towards alginate chains contingent upon the anions they are associated, thereby influencing the efficiency of crosslinking. Calcium acetate, derived from the weaker acid CH_3COOH, resulted in a higher pH level compared to calcium chloride, which originates from the strong acid HCL. In this context, calcium acetate displayed a stronger degree of ionization, thereby fostering crosslinking. Furthermore, calcium chloride, with its lower pH, introduced a greater number of hydrogen protons into the solution, leading to competitive interactions with the carboxylate functional groups and, consequently, reducing the crosslinking density. This can exert an influence on the overall ionic strength of the solution and subsequently affect the properties of the resulting gel, including its swelling behavior. The marginal discrepancies noted herein may be attributed to several factors, including the diffusion rate of calcium ions into the alginate polymer chain, the uniformity or heterogeneity in the distribution of calcium ions within the calcium chloride and acetate solutions, and potential issues related to clogging. Furthermore, the variations in experimental outcomes may also be ascribed to the potential presence of impurities within the reagents employed and the inherent variability encountered during experimentation.

In terms of the type of core-fiber effects on the hydrogel coating thickness, the results revealed considerable differences between PES and PVA, as higher hydrogel thickness was observed in PES. The differences can be due to fibers morphology, physical properties and chemical compositions. Regarding the physical differences between PES and PVA, the cross-section structures played a key role in the amount of hydrogel loaded on the core-fibers. PES is a multi-filament crimped yarn, wherein the PVA fiber is a mono-filament (Table 1). In addition, PES fibers have asymmetric crimped structures with nonuniform cross-section area over the length of the fibers, while PVA fibers have round and symmetrical cross-section structures, as observed in SME images (Fig. 3). PES fibers crimped structure provided a higher surface area for the prepolymer solution to adhere, leading to higher hydrogel coating thickness.

Further, the hydrogel penetrated the PES filament inter-spaces, supplying more hydrogel attachment. On the other hand, the PVA fibers with smooth surfaces provided less surface area and no opportunity for the hydrogel to interpenetrate into the mono-filament. However, the hydrogel thickness results indicated less variance in the PVA fiber than PES, which can be associated with the uniformity of PVA diameter along its length, resulting in a more uniform hydrogel coating. In Fig. 4, hydrogel coatings of PES and PVA fibers were cut to produce SEM images showing the interface between hydrogel and core-fibers. It was concluded that after completion of hydrogel crosslinking and drying, the hydrogel had higher interfacial interaction with PVA rather than PES. In terms of chemistry, both PES fibers are made of hydrophobic compounds, which decrease the compatibility with hydrophilic alginate. On the other hand, PVA fibers contain hydrophilic (hydroxyl group) and hydrophobic groups (acetate group), based on the degree of hydrolyzation during manufacturing. Based on SEM images shown in Fig. 4, PVA fibers indicated higher chemical compatibility with calcium-alginate hydrogel due to hydrophilicity of the hydroxyl groups, compared to lesser chemical compatibility observed in hydrophobic PES fibers.

In addition to hydrogel thickness, the weight of the loaded hydrogel on the core-fibers was calculated, as shown in Fig. 5. The significance of presenting the hydrogel weight normalized per length of the core-fibers was for the applications where the weight of hydrogel would be of higher priority than the thickness. In terms of self-healing, the mass of hydrogel controls the swelling ratio and the amount of loaded bio-self-healing agents on each unit length of the BioFibers. The trend of hydrogel weight change was similar to the thickness considering the Na-Alg concentration, crosslinker type, and the core-fiber materials.

3.2. Hydrogel swelling performance

The swelling capacity of the hydrogel-coated core-fibers was measured through gravimetric analysis and presented in Fig. 6 to Fig. 8. The effects of Na-Alg concentration, cation crosslinker type, time of exposure to the solution, and pH of the solution were investigated. The results revealed that the hydrogel crosslinked with higher Na-Alg concentration and CA showed a higher swelling ratio (Fig. 6) since a higher weight of hydrogel was loaded on the core-fibers in these conditions. For instance, the core-fibers coated with 8 w/v Na-Alg crosslinked with CA showed a swelling ratio (g/g) of 7.14 for PES and 4.41 for PVA, as the samples were exposed to DI water for 15 min. These results revealed that the swelling ratio of crosslinked alginate can be mainly tailored by using different prepolymer concentrations. In Fig. 7, the effects of time of exposure on the swelling ratio of the hydrogel was studied under time interval of 5, 10, 15, and 30 min. The samples with crosslinked hydrogel using 8 w/v Na-Alg and CA were employed for this parametric study. The results also indicated that the swelling ratios increased as the exposure time increased to 10 min. The swelling ratios reached a plateau after 10 min of exposure, indicating that the polymer chain arrived at

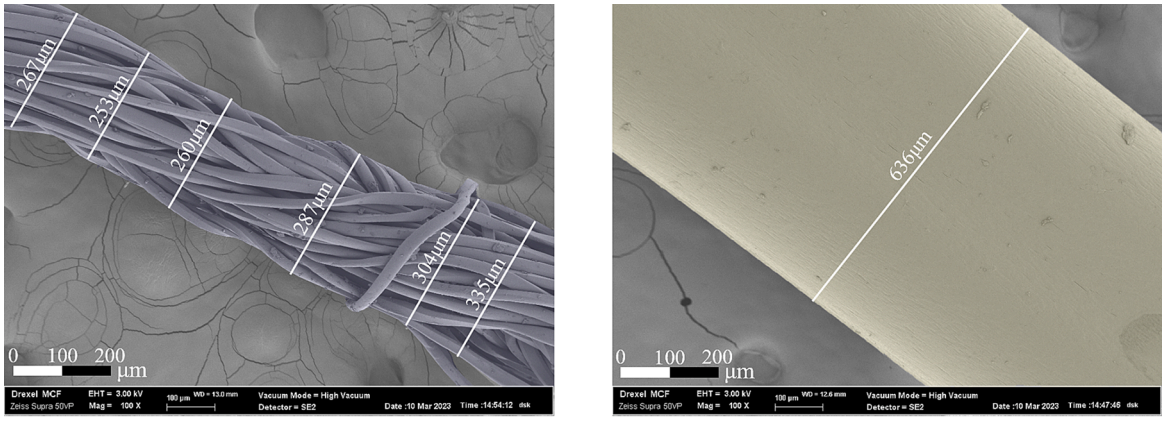

(a) (b)

Fig. 3. SEM images of the core-fiber without hydrogel coating: (a) PES, (b) PVA (It should be noted that the SEM images featured in this manuscript were enhanced with colorization to improve the visual presentation).

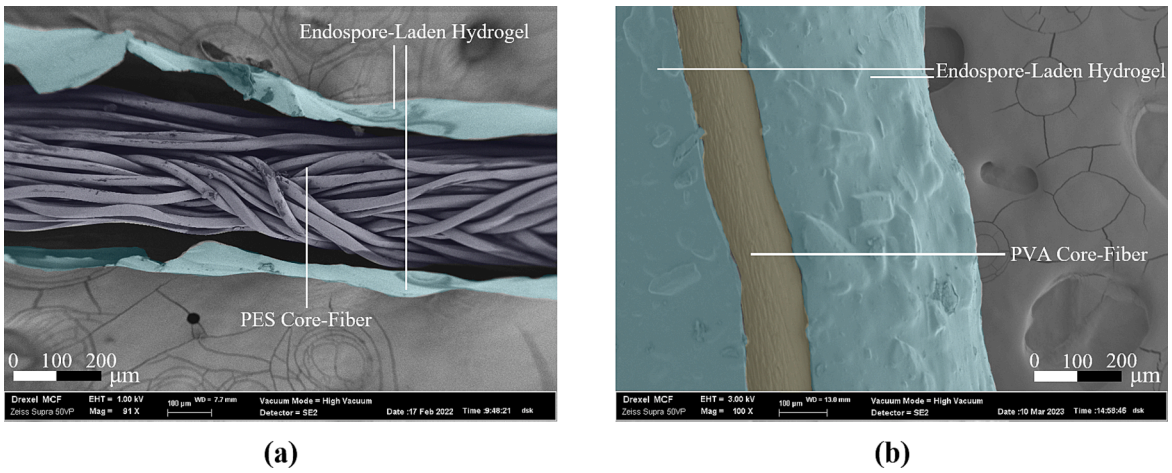

Fig. 4. SEM images of the core-fiber with hydrogel coating (2 w/v Na-Alg with CC): (a) PES, (b) PVA.

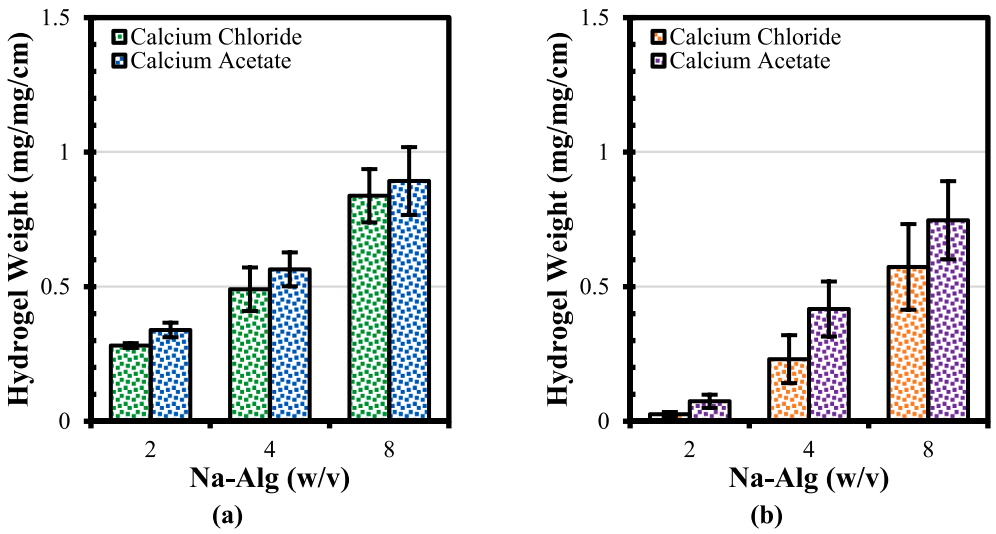

Fig. 5. Hydrogel coating weight (mg) per unit length of core-fiber (cm): (a) PES, (b) PVA (the statistic shown this plot is based on 30 replicates for each set of samples).

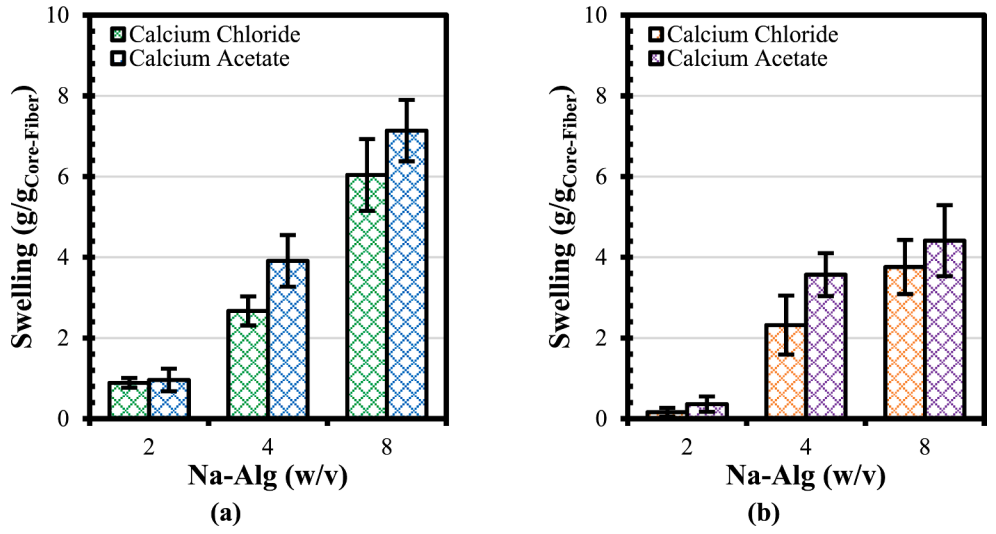

Fig. 6. Hydrogel swelling ratio exposed to the DI water for 15 min (a) PES, (b) PVA (g/g$_{Core-Fiber}$ in y-axis indicates the weight of solution, in grams, absorbed per weight of the BioFiber as described in Eq. (4) (the statistic shown this plot is based on 10 replicates for each set of samples).

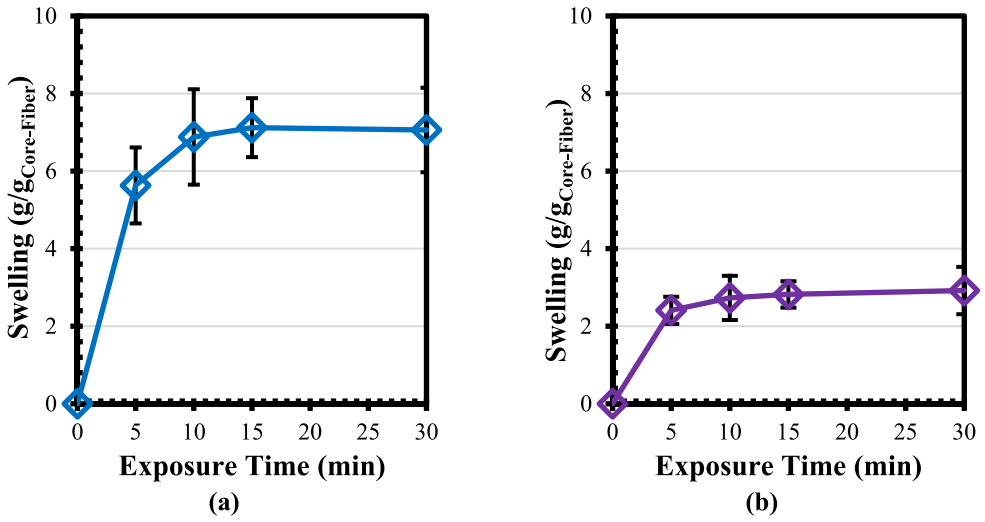

Fig. 7. Hydrogel swelling ratio for 8 w/v Na-Alg crosslinked with CA, exposed to the DI water (a) PES, (b) PVA (the statistic shown this plot is based on 10 replicates for each set of samples).

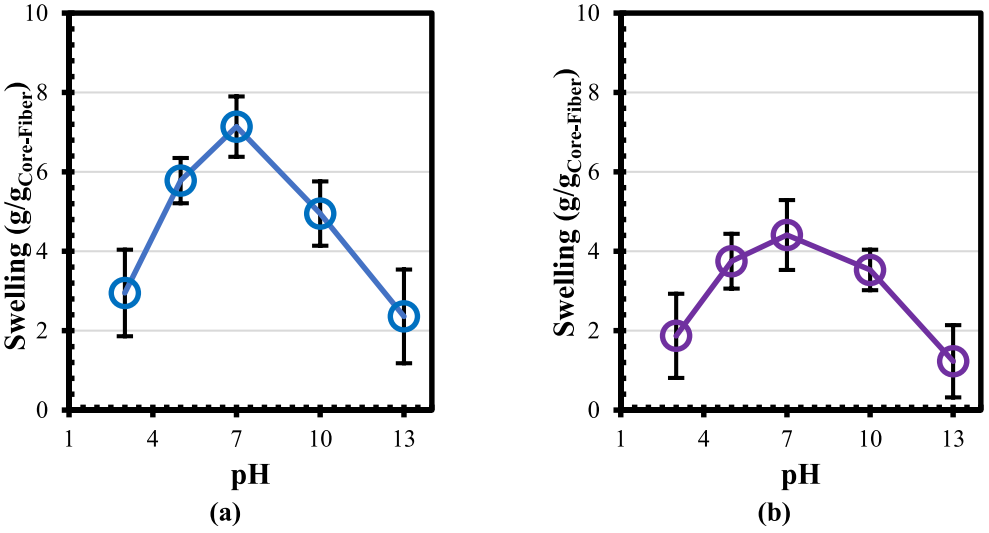

Fig. 8. Hydrogel swelling ratio for 8 w/v Na-Alg crosslinked with CA, with 15 min exposure (a) PES, (b) PVA (the statistic shown this plot is based on 10 replicates for each set of samples).

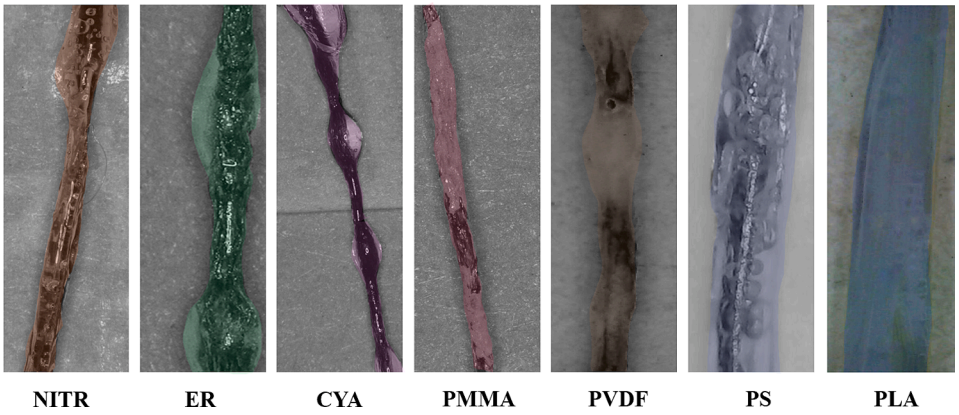

Fig. 9. Examples of shell coating materials on hydrogel coated core-fibers (It should be noted that the images underwent colorization to accentuate the specific features of the BioFiber, showcasing the distinct shell coatings).

the maximum liquid absorption capacity. Since the crosslinked alginate swelling capacity is pH sensitive, a parametric study was conducted using acidic, neutral, and basic aqueous solutions with pH of 3, 5, 7, 10, and 13. Ethanoic acid (CH_3COOH) was used as a solution with acidic pH, and sodium/potassium hydroxide solution was used for synthesizing basic pH. Fig. 8 displays the variation of hydrogel swelling ratio as the pH of the exposed solution shifted towards acidic or basic solutions. Under acidic conditions, the limited expansion ratio can be attributed to the strong repulsion between anion-anion COO– groups. However, in basic conditions (specifically, when a synthesized pore solution is present), the presence of counter ions (Na + and K +) and non-ionic hydrophilic OH– can lead to a reduction in swelling.

3.3. Shell coating morphology

For the final fiber shell coating (on the hydrogel sheath), several polymeric materials were studied to confirm shell materials can meet: (i) desirable coating layer morphology in terms of low coating-to-fiber ratio and uniformity, (ii) impermeability to protect endospore-laden hydrogel from undesired access to moisture/aqueous solution, (iii) and abrasion resistance during blending with the target quasi-brittle matrix. To shortlist the shell material, a shell coating with a uniform coating and a low coating-to-fiber ratio was explored. The visual observations of the BioFibers manufactured using the candidate polymers are illustrated in Fig. 9. It was observed that most of the shell material options failed in terms of coating uniformity, except for the PS and PLA. PS and PLA are both non-polar and hydrophobic polymers. PS is a brittle polymer while PLA is a relatively flexible polymer; accordingly, a blend of PS-PLA co-polymer was studied to tune flexibility/brittleness of the shell coating.

For PS/PLA polymer blend, a mass ratio of 1:1 was selected in this study. The 1:1 wt% polymers blend ratio was determined through an iterative process involving trial and error, whereby different values were tested and assessed to identify the optimal selection based on initial fluid ingress and abrasion survivability tests. A parametric study was conducted using 6, 12, and 18 w/v of copolymer/solvent ratio to explore the effect of copolymer solution viscosity on the shell coating thickness. Moreover, the number of shell layers applied on the core-fibers varied from 1 to 5 layers to tune the thickness and impermeability. Core-fibers coated with hydrogel crosslinked with 8 w/v Na-Alg and CA were selected and used in this section as they provided higher hydrogel coating and swelling capacity. Fig. 10 and Fig. 11 present the visual observations of the shell coating with different copolymer/solvent ratio and number of applied layers on PES and PVA core-fibers. These figures indicated that the shell coating was more uniformly adhered to PVA fiber compared to PES. This observation was mainly attributed to the rigidity of the PVA core-fiber being higher than PES core-fiber. During shell coating, the rigidity of the core-fiber was found to favor the coating process, resulting in evenly distributed shell materials on the fibers.

Fig. 12 shows the average and standard deviation of BioFiber diameters as copolymer/solvent and number of coating layers changed. The results revealed that a lower copolymer/solvent ratio led to a lower shell coating thickness. This was due to a lower viscosity in the shell polymer solution made using a polymer with lower molecular weights, which resulted in a lower amount of polymer adhering to the hydrogel coated core-fibers. In terms of the added thickness by the shell coating, an average of each layer of shell coating was plotted in Fig. 13. This result showed that the shell coating on PES led to higher thickness per layer, compared to PVA. Notably, the PVA core-fiber is a single filament, while PES is a multi-filament with greater diameter variability along its length. This variability in PES diameter resulted in a more pronounced fluctuation in coating thickness in both the hydrogel and shell coating when compared to PVA core-fiber. For instance, the 18 w/v copolymer solution added an average of 23.20 % thickness per shell layer since this value went up to 32.01 % for PES. In addition, the PVA shell coating showed less thickness variation compared to PES.

3.4. Fluid ingress survivability test

To study the shell coating thickness on the hydrogel/PVA fibers for impermeability, 1 to 5 coating layers of PLA:PS co-polymer (1:1 mass blend with 12 w/v copolymer/solvent ratio) were applied. For this section, the alginate concentration kept constant at 8 wt% as it provided the highest swelling capacity in the hydrogel. The results of fluid ingress survivability for 1- and 2-hour(s) exposure to a basic solution (pH of ~ 13) were shown in Table 5. In this table, the results are presented as failed/passed, indicating that the BioFibers with the minimum diameter and shell coating survived the fluid ingress test.

The morphology observation of PLA:PS coatings on core-fibers are

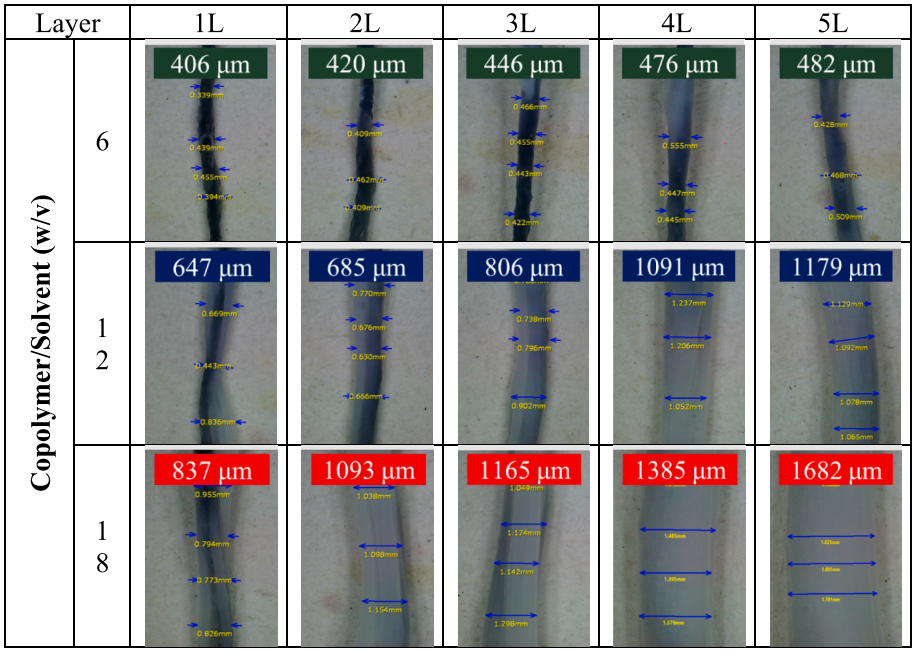

Fig. 10. Average shell coating thickness on PES using PLA:PS (1:1 wt%) (the statistic shown this plot is based on 10 replicates for each set of samples).

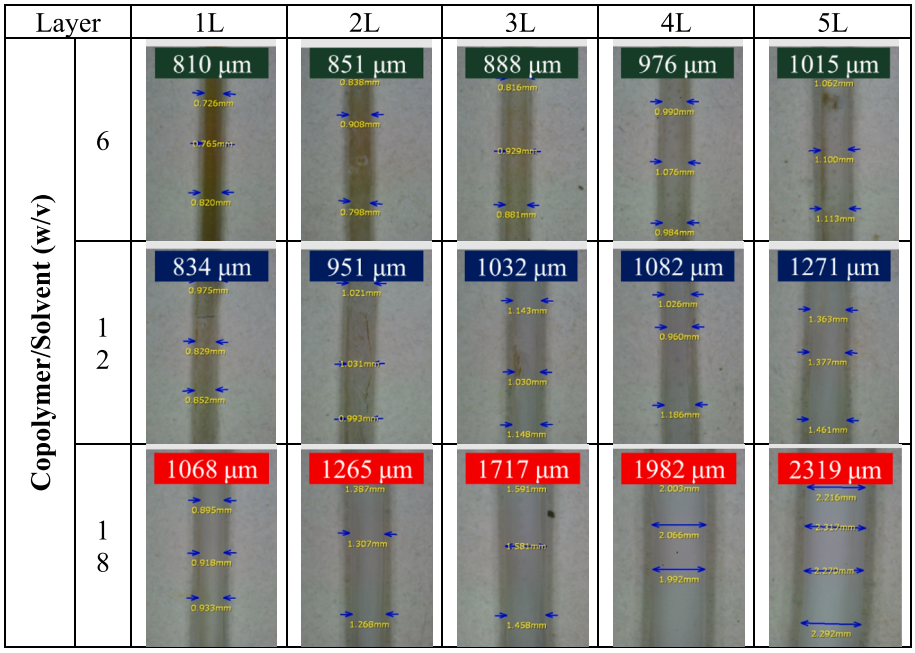

Fig. 11. Average shell coating on PVA using PLA:PS (1:1 wt%) (the statistic shown this plot is based on 10 replicates for each set of samples).

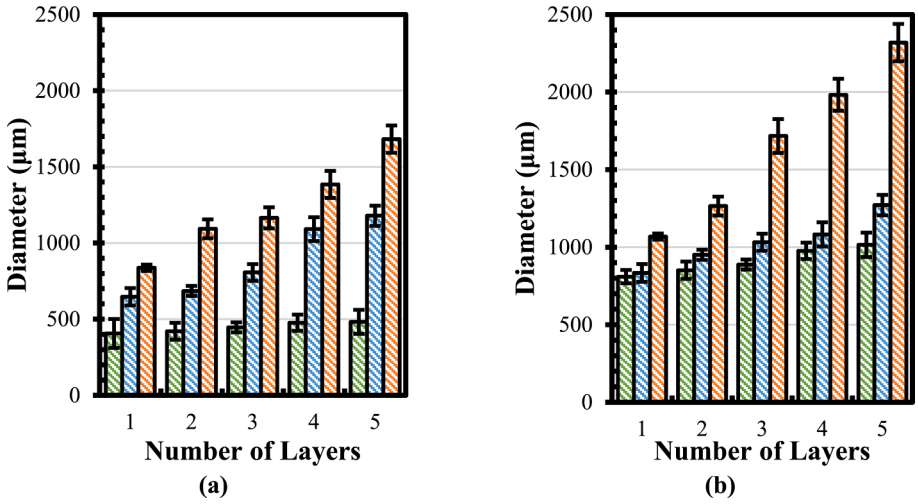

Fig. 12. Shell coating thickness using PLA:PS (1:1 wt%) (a) PES, (b) PVA (the statistic shown this plot is based on 10 replicates for each set of samples).

shown in Fig. 14 and Fig. 15. These SEM pictures indicated the pore appearance in different copolymer/solvent and the number of layers. Fig. 14 indicates the one-layer coating of 6 w/v PLA:PS on the PVA; various pores with sizes in the range of 1–3 µm were observed on the shell coating. The observed porous structure can be associated with solvent evaporation at ambient conditions leading to formation of three-dimensional porous films. On the other hand, the SEM pictures shown in Fig. 15 revealed that less porous structures were formed in the case of 1-layer 18 w/v PLA:PS shell. Indeed, 18 w/v PLA:PS contains higher polymer and lesser solvent than 6 w/v PLA:PS and accordingly, more polymers can serve as building blocks leading to formation of less porous structure. The porous structure can adversely impact the shell survivability against the fluid ingress.

3.5. Shell abrasion resistance

This study used the manufacturing process (i.e., shear or manual mixing) of the quasi-brittle cementitious composite as a method to determine the abrasion resistance of shell coating against manual and mechanical shear mixing. The abrasion survivability results were plotted in Fig. 16 for PES and PVA core-fibers. It was concluded that the lower number of BioFibers survived mechanical shear mixing (MSM) compared to manual mixing (MM). This was due to higher stress applied on the shell coating in the case of mechanical mixing done by a vacuum mixer. Further, it was observed that the BioFibers made with PVA showed a higher survivability rate compared to PES. This was mainly associated with the difference in rigidity of core-fibers. The high rigidity of the core-fiber, i.e., PVA, was beneficial during the mixing stage as it resisted higher deformation. In terms of the copolymer/solvent ratio, PES with 12w/v-5L, and PVA with 18-2L showed higher survivability rates.

3.6. MICCP activity

Thermogravimetric analysis (TGA) was performed to quantitatively analyze the precipitation of calcium carbonate in the activated BioFibers

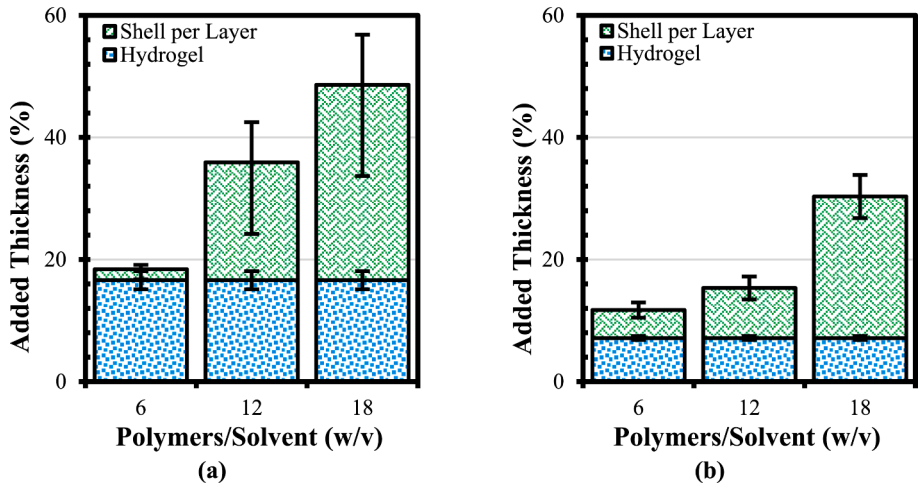

Fig. 13. The percentage of added thickness when one layer of hydrogel/shell was applied to the core-fiber (a) PES, (b) PVA.

Table 5
Shell coating survivability against ingress of aqueous solution.

		PES		PVA	
w/v	Layer	1 hr	2 hr	1 hr	2 hr
6	1	F	F	F	F
	2	F	F	F	F
	3	F	F	F	F
	4	F	F	P	F
	5	F	F	P	F
12	1	F	F	F	F
	2	P	F	P	F
	3	P	F	P	F
	4	P	P	P	F
	5	P	P	P	P
18	1	P	F	P	F
	2	P	P	P	P
	3	P	P	P	P
	4	P	P	P	P
	5	P	P	P	P
Required $D_{BioFiber}$ (um)		680	1090	950	1080
Required t_{Shell} (%)		35	86	18	28

F: Failed.
P: Passed.
$D_{BioFiber}$: Total diameter of the fiber after hydrogel and shell coatings.
t_{Shell}: Shell thickness as defined in section 2.3.1.

to evaluate the self-healing capacity. BioFibers activation was achieved by delinquently cracking only shell coating using a surgical knife and microscope and then, exposing BioFibers to activation media. This activation method was applied to the BioFibers to have a controlled and consistent activation for all the samples. Upon exposure, endospores were released to the media where they can reach the nutrient, germinate, and accordingly produce carbonate ions. Carbonate ions can then react with calcium available in the media and MICCP can be achieved. For TGA test, a total of 24 tests were performed on intact and fractured BioFiber made with 8 w/v Na-Alg and PS:PLA (1:1 mass%). For shell coating, PES coated with 12 w/v-5L copolymer/solvent, and PVA with 18 w/v-1L copolymer/solvent were used. After MICCP was terminated, BioFibers were separated from solid residue, and TGA tests were conducted on residue solid mineral powder. Fig. 17 presented weight loss curves (TGA) and derivative curves (DTG) showcasing TGA results for both intact and fractured BioFibers, providing a selection of data for analysis. In TGA results, several weight losses were observed. The weight loss in the temperature range of 30–105 °C was mainly attributed with moisture loss in the samples and the weight loss between 200 and 600 °C was mainly attributed with the organic matter decomposition into residue solid and gases [67]. The weight loss in the temperature range of 600–800 °C was mainly attributed to the decomposition of calcium carbonate ($CaCO_3$) to calcium oxide (CaO) [68]. Calculation of the quantity of calcium carbonate was performed utilizing the following equations:

$$W_{CaCO_3}(\%) = \left[WL_{CaCO_3} \times (M_{CaCO_3}/M_{CO_2})\right] \Big/ (W_{Int} - W_W) \quad (5)$$

$$W_{CaCO_3}(mg) = W_{CaCO_3}(\%) \times W_{Res} \quad (6)$$

where WL_{CaCO3} is the weight loss between 600 and 800 °C, M_{CaCO3} and M_{CO2} are the molar weight of calcium carbonate and carbon dioxide. In order to remove the moisture in the results, the normalized weight of $CaCO_3$, i.e., W_{CaCO3}(%), was calculated using the initial weight of the TGA sample (W_{Int}) subtracted by the weight loss associated with the moisture loss (W_W). To determine the amount of calcium carbonate precipitated by each BioFiber, the weight percentage of $CaCO_3$ in each TGA test was multiplied by the weight of solid residue after MICCP (W_{Res}).

In Fig. 18, the results for quantified amount of $CaCO_3$ were shown for intact and fractured BioFibers. The intact BioFibers were used as control samples to determine the difference between precipitation in pre-activated and post-activated BioFibers. The results indicated that the fractured BioFibers produced significant calcium carbonate compared to intact samples. Although it was anticipated that the intact BioFiber would exhibit no precipitation of calcium carbonate, a small quantity was detected. This occurrence can be attributed to imperfections present at the edges of the BioFibers or the introduction of external contaminants, i.e., urease-producing bacterial species, during the manufacturing process of the shell coating. These results demonstrate that the BioFibers can produce self-healing MICCP products after activation. Whereas little self-healing MICCP activity was relatively observed in intact BioFibers. The negligible to zero MICCP activity in intact BioFibers implies that the developed shell coating can protect the endospores from releasing into the media before damage occurrence, supporting the damage-responsiveness functionality of the developed BioFibers.

In addition to TGA results, SEM images were taken from the fractured BioFibers before and after MICCP activation. As it is shown in Fig. 19(a), no mineral formation was observed in BioFibers before MICCP activation. Whereas, SEM images, shown in Fig. 19(b), revealed formation of minerals adjacent to the fractured zone after MICCP activation. The mineral formation initiated by hydrogel swelling and endospores releasing into the media. Afterwards, the solid MICCP residues were detected on the core-fibers and the detached shell layers. These

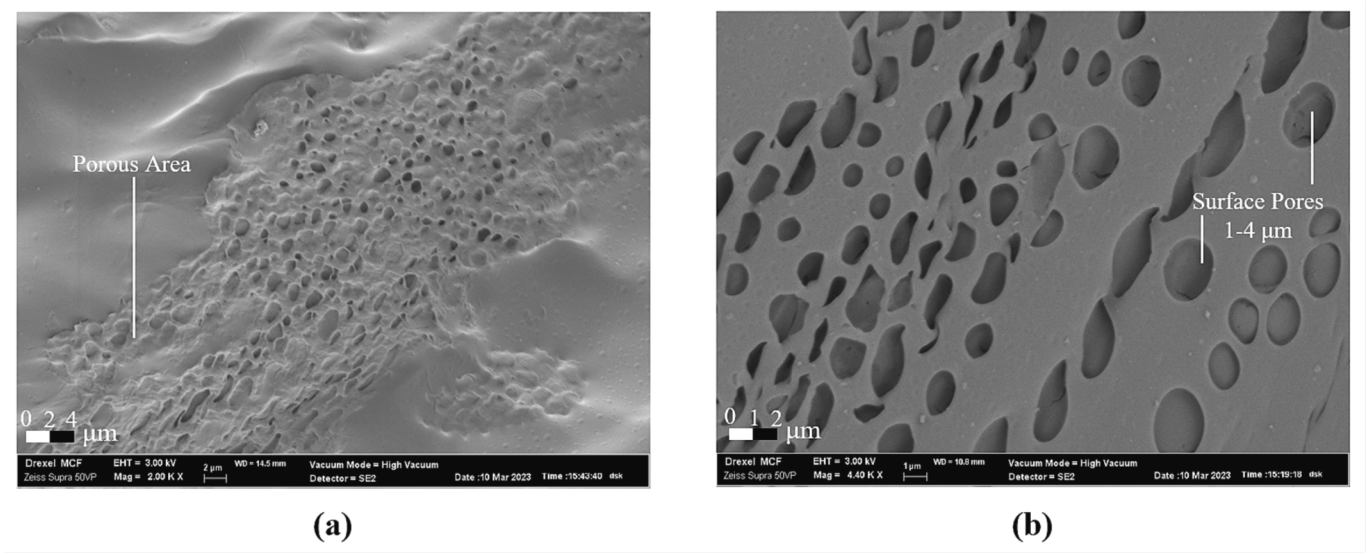

Fig. 14. SEM images of the core-fiber coated with hydrogel and shell (PLA:PS 6w/v, 1-layer): (a) 2.00 kX, (b) 4.40 kX.

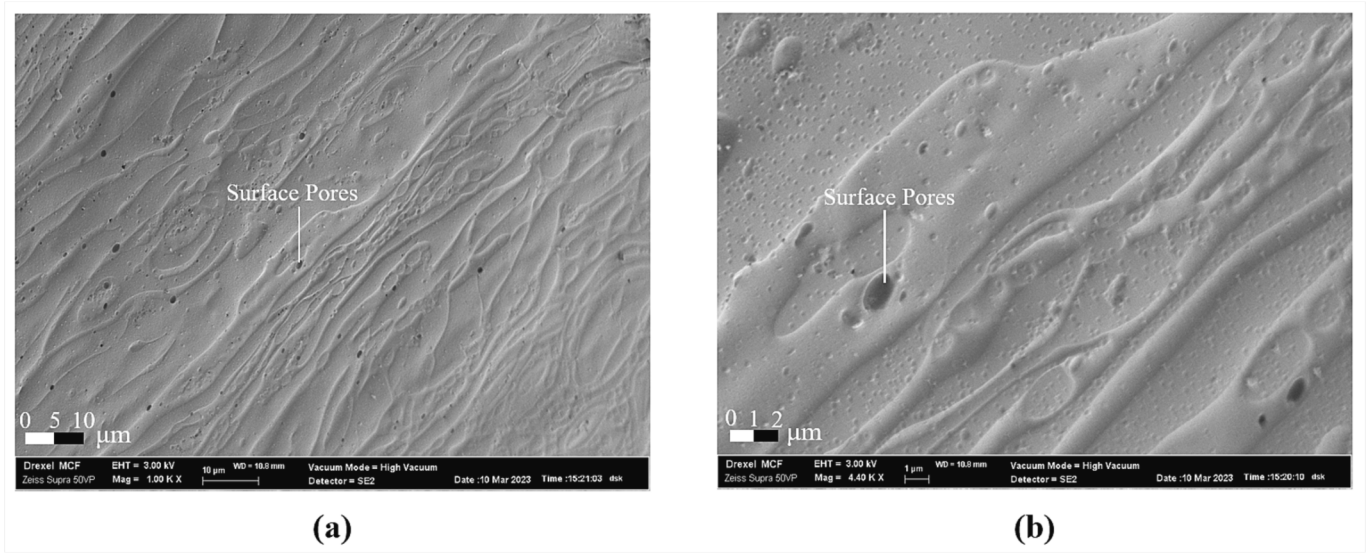

Fig. 15. SEM images of the core-fiber coated with hydrogel and shell (PLA:PS 18w/v, 1-layer): (a) 2.00 kX, (b) 4.40 kX.

observations also acknowledge the mineral formation capacity of the developed BioFibers prior to activation.

4. Summary and conclusion

This study investigated the development and self-healing performance of innovative multi-functional bacterial-based polymeric-based fibers, titled BioFibers, in quasi-brittle cementitious composites. BioFibers developed to provide three primary functionalities: (i) autonomous MICCP self-healing, (ii) crack growth control, and (iii) damage-responsiveness. Based on the results obtained in this study, following conclusions can be drawn:

- The crosslinked alginate demonstrated its ability to function as a carrier for endospore, providing high endospore survivability rate and sufficient swelling capacity for MICCP. Additionally, it was observed that increasing the concentration of sodium-alginate resulted in greater amounts of hydrogel being loaded onto the core-fiber, leading to higher swelling capacity and higher endospore concentrations in the BioFibers. Through a parametric study, it was determined that deviations from neutral pH caused a decrease in the hydrogel swelling ratio, up to 57 % for acidic and 72 % for basic conditions.
- The incorporation of the polystyrene/polylactic acid copolymer shell coating successfully introduced the necessary damage-responsive characteristic to the BioFibers. The copolymer coating functioned as a protective barrier, preventing the release of endospores prior to the occurrence of cracks. The thickness of the hydrogel and shell coating was tailored to achieve the minimum value that meets the performance requirements, i.e., hydrogel high swelling and shell survivability against fluid ingress.
- The polymer blend (1:1 wt%) of polylactic acid and polystyrene dissolved in chloroform provided proper shell coating for BioFibers in terms of uniformity. Different copolymer/solvent ration resulted in different shell coating ratio, affecting the shell survivability against fluid ingress and mechanical forces applied during mixing with the matrix. A shell thickness of 35 and 18 % were required to pass 1 h fluid ingress survivability test on the PES and PVA core-fiber,

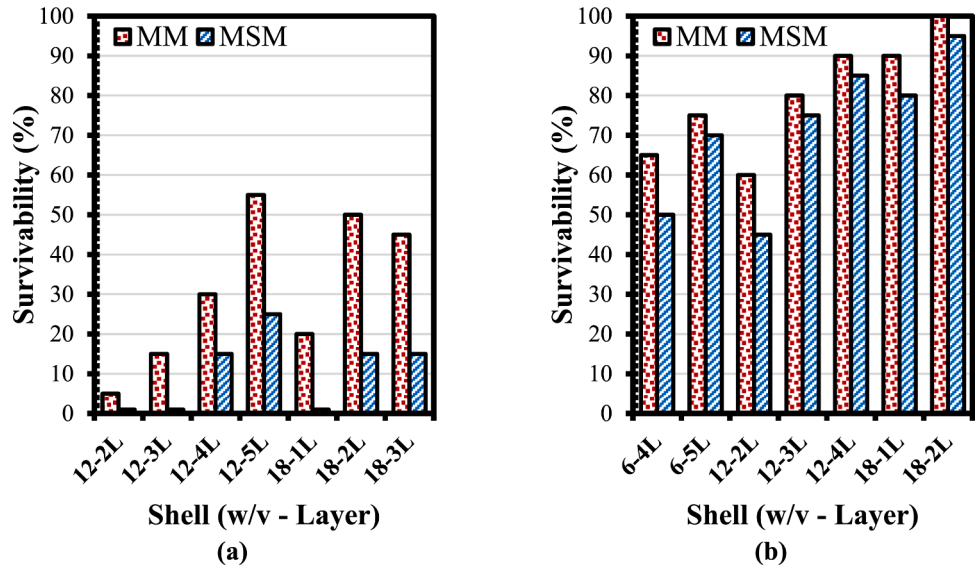

Fig. 16. BioFiber with core-fiber (a) PES, (b) PVA survivability test results against casting mechanical forces for different shell coating (copolymer/solvent ratio as w/v and number of applied coatings as L) (Note that survivability is defined as the number of BioFibers remained intact after simulated casting process with respect to the total number of used BioFiber).

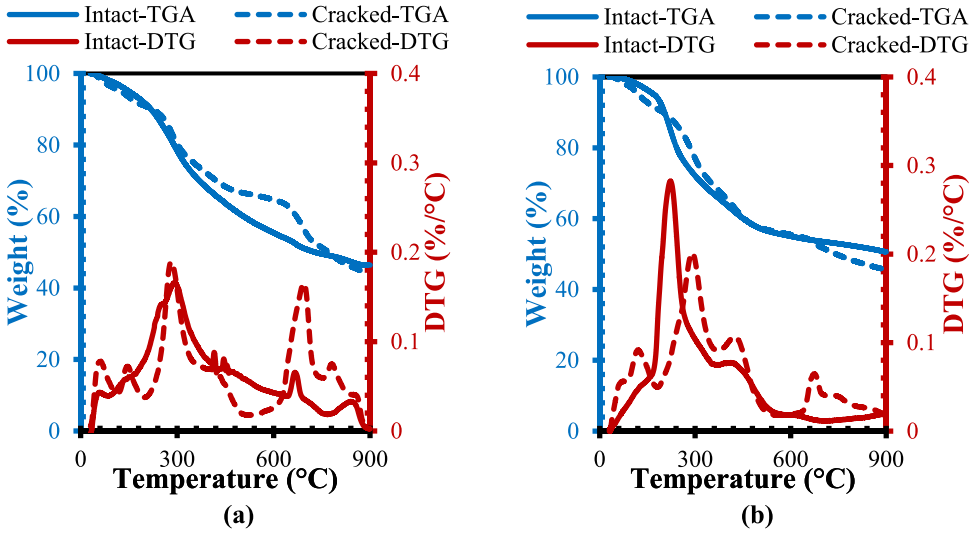

Fig. 17. A set of representative thermogravimetric analysis results for BioFiber made of (a) PES, (b) PVA.

respectively. For simulated concrete casting, PVA with 18 w/v, 1-layer provided more abrasion resistance, 90 and 80 % survivability under hand and mechanical mixing, respectively.

- BioFiber MICCP activities were investigated quantitatively and qualitatively using thermogravimetric analysis and electron microscopy, respectively. The TGA results revealed that 32.5 and 19.4 % of total precipitated solid were calcium carbonate in the PES and PVA BioFiber, respectively. The precipitations obtained only after 30 h of BioFiber activation, which was mainly governed by the germination phase of endospores. In terms of total weight of precipitated calcium carbonate, 83.1 and 48.7 mg of calcium carbonate were produced per each BioFiber with PES and PVA core-fiber, respectively.
- The properties of core-fiber, including its morphology, stiffness, and chemical composition, can significantly influence BioFiber physical characteristics such as density, swelling capacity, and casting survivability. It was observed that PES BioFiber exhibited a higher quantity of calcium carbonate during the initial 30 h of activation compared to PVA BioFiber. However, in the long-term, the quantity of calcium carbonate is expected to reach a plateau, with similar values for both cases. This phenomenon occurs because the MICP process terminates once all the calcium and urea sources are depleted. Conversely, PVA BioFiber may exhibit better compatibility with concrete, as it tends to have a higher survivability during the concrete casting process and can contribute to a crack-bridging effect after the concrete hardening stage.

The current study has shown promising results in the performance of BioFibers. However, further research is necessary to assess how BioFibers integrate with cementitious matrix. It is crucial to understand the mechanical, fracture, bridging, and activation mechanisms of BioFibers to achieve the desired mechanical and physical properties of reinforced concrete. Balancing the fracture processes between the concrete, fiber shell, and fiber core, as well as managing MICCP activity and crack volume creation, is essential. Additionally, the crystal morphology of precipitated calcium carbonate plays a significant role in determining the self-healing efficiency of BioFibers, including factors like lattice

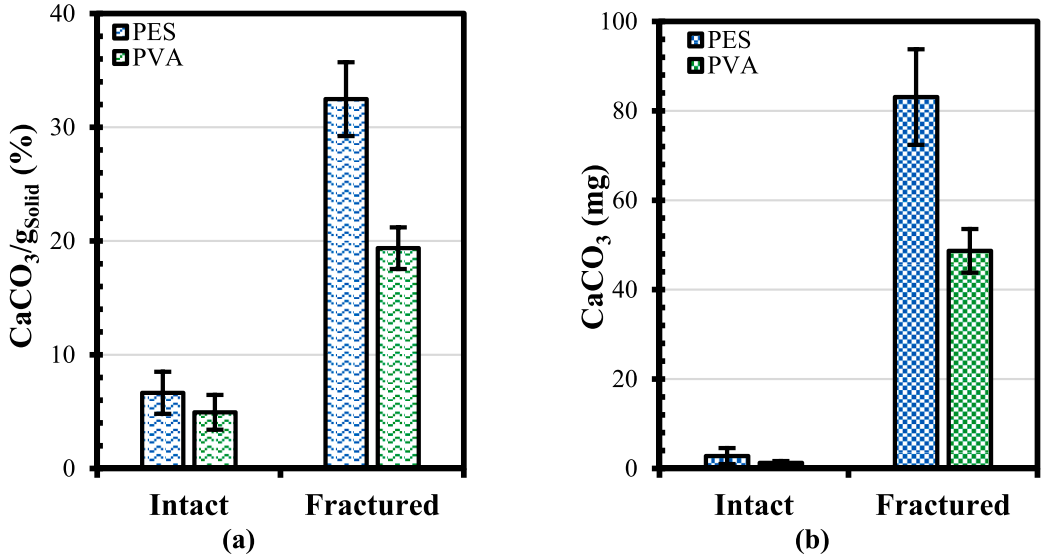

Fig. 18. Calcium carbonate quantification for intact and fractured (a) amount of calcium carbonate (in percentage) normalized to the total weight of tested samples, (b) total amount of calcium carbonate (in mg) precipitated per one BioFiber (the statistic shown in this plot is based on five replicates for each set of samples).

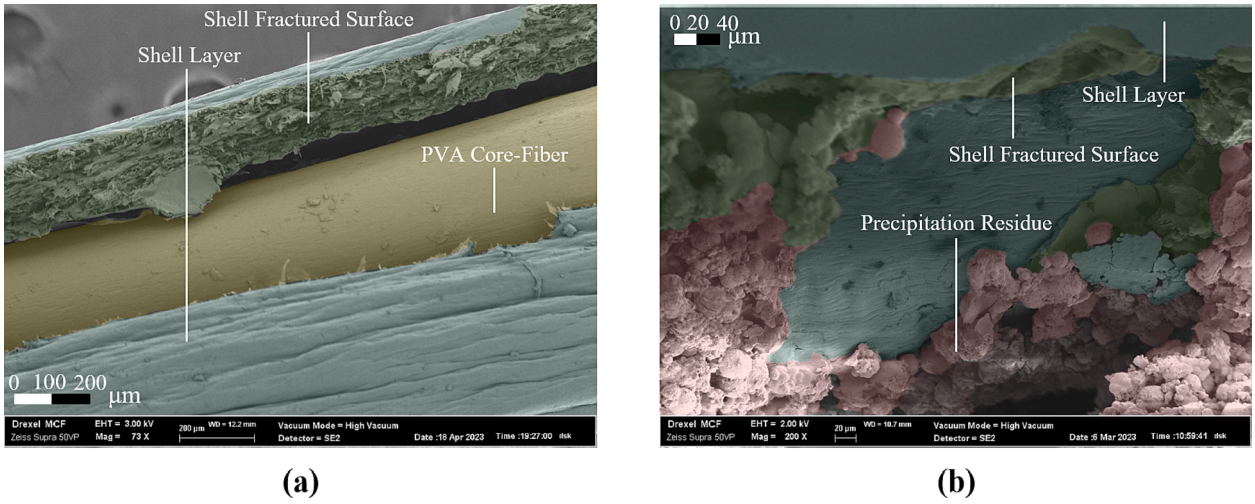

Fig. 19. SEM images of the fractured BioFiber (a) before MICCP, (b) after MICCP.

structure, distribution, and particle size. Another important aspect to explore in future studies is the sealing and healing mechanisms of concrete reinforced with BioFibers. This investigation will evaluate the effectiveness and robustness of the proposed approach, as well as the potential enhancement of durability and resilience in fractured concrete.

CRediT authorship contribution statement

Mohammad Houshmand Khaneghahi: Writing – original draft, Writing – review & editing, Validation, Methodology, Investigation, Data curation, Visualization, Conceptualization, Formal analysis, Software. **Divya Kamireddi:** Writing – review & editing, Validation, Methodology, Investigation, Data curation. **Seyed Ali Rahmaninezhad:** Writing – review & editing, Methodology, Investigation. **Amirreza Sadighi:** Writing – review & editing, Methodology, Investigation. **Caroline L. Schauer:** Supervision, Resources, Methodology, Funding acquisition, Conceptualization. **Christopher M. Sales:** Writing – review & editing, Supervision, Resources, Methodology, Funding acquisition, Conceptualization. **Ahmad R. Najafi:** Supervision, Funding acquisition, Conceptualization, Writing – review & editing. **Aidan Cotton:** Visualization, Investigation. **Reva Street:** Supervision, Resources, Methodology. **Yaghoob (Amir) Farnam:** Writing – review & editing, Methodology, Investigation, Supervision, Resources, Funding acquisition, Conceptualization, Validation, Project administration.

Declaration of Competing Interest

The authors declare that they have no known competing financial interests or personal relationships that could have appeared to influence the work reported in this paper.

Data availability

Data will be made available on request.

Acknowledgement

The work presented here has been supported by the National Science Foundation (NSF CMMI – 2029555) and was performed at Drexel University in the Advanced and Sustainable Infrastructure Materials (ASIM) Lab. Any opinions, findings, and conclusions or recommendations expressed in this material are those of the authors and do not necessarily reflect the views of the National Science Foundation.

References

[1] N.I. Khan, S. Halder, Self-healing fiber-reinforced polymer composites for their potential structural applications, in: Self-Healing Polymer-Based Systems, Elsevier, 2020, pp. 455–472.
[2] H. Pulikkalparambil, et al., Self-repairing hollow-fiber polymer composites, Self-Healing Composite Materials (2020) 313–326.
[3] P.W. Beaumont, et al., Comprehensive composite materials II, Elsevier Amsterdam, The Netherlands, 2018.
[4] F. Althoey, M. Balapour, Y. Farnam, Reducing detrimental sulfate-based phase formation in concrete exposed to sodium chloride using supplementary cementitious materials, Journal of Building Engineering 45 (2022), 103639.
[5] C. Laschi, B. Mazzolai, Bioinspired materials and approaches for soft robotics, MRS Bull. 46 (2021) 345–349.
[6] P.K. Jogi, T.V. Lakshmi, Self healing concrete based on different bacteria: a review, Mater. Today:. Proc. 43 (2021) 1246–1252.
[7] S. Terryn, et al., Toward self-healing actuators: A preliminary concept, IEEE Trans. Rob. 32 (3) (2016) 736–743.
[8] M. Ksara, et al., Microbial damage mitigation strategy in cementitious materials exposed to calcium chloride, Constr. Build. Mater. 195 (2019) 1–9.
[9] S. Zwaag, Self healing materials: an alternative approach to 20 centuries of materials science, Springer Science+ Business Media BV Dordrecht, The Netherlands, 2008.
[10] K.W. Shah, G.F. Huseien, Biomimetic self-healing cementitious construction materials for smart buildings, Biomimetics 5 (4) (2020) 47.
[11] M.B. Witte, A. Barbul, General principles of wound healing, Surg. Clin. N. Am. 77 (3) (1997) 509–528.
[12] H.N. Wilkinson, M.J. Hardman, Wound healing: cellular mechanisms and pathological outcomes, Open Biol. 10 (9) (2020), 200223.
[13] J. He, C. Qiao, Y. Farnam, Durability evaluation of reinforced concrete with surface treatment of soy methyl ester-polystyrene under freeze-thaw cycles and calcium chloride, Cem. Concr. Compos. (2023), 104927.
[14] F. Althoey, et al., Thermo-chemo-mechanical understanding of damage development in porous cementitious materials exposed to sodium chloride under thermal cycling, Cem. Concr. Res. 147 (2021), 106497.
[15] I. De Luca, et al., Nanotechnology development for formulating essential oils in wound dressing materials to promote the wound-healing process: a review, Appl. Sci. 11 (4) (2021) 1713.
[16] P.-H. Lin, et al., Zinc in wound healing modulation, Nutrients 10 (1) (2017) 16.
[17] R. Narayan, et al., Self-healing: an emerging technology for next-generation smart batteries, Adv. Energy Mater. 12 (17) (2022) 2102652.
[18] E.J. Barbero, F. Greco, P. Lonetti, Continuum damage-healing mechanics with application to self-healing composites, Int. J. Damage Mech 14 (1) (2005) 51–81.
[19] J. Ekeocha, et al., Challenges and opportunities of self-healing polymers and devices for extreme and hostile environments, Adv. Mater. 33 (33) (2021) 2008052.
[20] C.E. Diesendruck, et al., Biomimetic self-healing, Angew. Chem. Int. Ed. 54 (36) (2015) 10428–10447.
[21] D.Y. Wu, S. Meure, D. Solomon, Self-healing polymeric materials: a review of recent developments, Prog. Polym. Sci. 33 (5) (2008) 479–522.
[22] R.P. Wool, Self-healing materials: a review, Soft Matter 4 (3) (2008) 400–418.
[23] M.D. Hager, et al., Self-healing materials, Adv. Mater. 22 (47) (2010) 5424–5430.
[24] P. Dinarvand, A. Rashno, Review of the potential application of bacteria in self-healing and the improving properties of concrete/mortar, J. Sustainable Cem.-Based Mater. 11 (4) (2022) 250–271.
[25] K. Chetty, et al., Self-healing bioconcrete based on non-axenic granules: a potential solution for concrete wastewater infrastructure, J. Water Process Eng. 42 (2021), 102139.
[26] M. Fahimizadeh, et al., Multifunctional, sustainable, and biological non-ureolytic self-healing systems for cement-based materials, Engineering (2022).
[27] S.C. Chuo, et al., Insights into the current trends in the utilization of bacteria for microbially induced calcium carbonate precipitation, Materials 13 (21) (2020) 4993.
[28] Rahmaninezhad, S.A., et al., Evaluation of different strategies for efficient sporulation and germination of the MICP bacterium Lysinibacillus sphaericus strain MB284 (ATCC 13805). bioRxiv, 2022: p. 2022.09. 15.508202.
[29] E.P. Riley, et al., Milestones in Bacillus subtilis sporulation research, Microbial Cell 8 (1) (2021) 1.
[30] G. Souradeep, H.W. Kua, Encapsulation technology and techniques in self-healing concrete, J. Mater. Civ. Eng. 28 (12) (2016) 04016165.
[31] J. Wang, et al., Self-healing concrete by use of microencapsulated bacterial spores, Cem. Concr. Res. 56 (2014) 139–152.
[32] Y. Tang, J. Xu, Application of microbial precipitation in self-healing concrete: a review on the protection strategies for bacteria, Constr. Build. Mater. 306 (2021), 124950.
[33] N. De Belie, et al., A review of self-healing concrete for damage management of structures, Adv. Mater. Interfaces 5 (17) (2018) 1800074.
[34] S. Sangadji, Can self-healing mechanism helps concrete structures sustainable? Procedia Eng. 171 (2017) 238–249.
[35] Z. Wan, et al., Mechanical properties and healing efficiency of 3D-printed ABS vascular based self-healing cementitious composite: experiments and modelling, Eng. Fract. Mech. 267 (2022), 108471.
[36] C. De Nardi, D. Gardner, A.D. Jefferson, Development of 3D printed networks in self-healing concrete, Materials 13 (6) (2020) 1328.
[37] K. Vijay, M. Murmu, S.V. Deo, Bacteria based self healing concrete–A review, Constr. Build. Mater. 152 (2017) 1008–1014.
[38] M. Alazhari, et al., Application of expanded perlite encapsulated bacteria and growth media for self-healing concrete, Constr. Build. Mater. 160 (2018) 610–619.
[39] X. Zhu, et al., Viability determination of Bacillus sphaericus after encapsulation in hydrogel for self-healing concrete via microcalorimetry and in situ oxygen concentration measurements, Cem. Concr. Compos. 119 (2021), 104006.
[40] F. Althoey, et al., Physical, strength, durability and microstructural analysis of self-healing concrete: a systematic review, Case Stud. Constr. Mater. 18 (2023) e01730.
[41] G.F. Huseien, et al., Smart bio-agents-activated sustainable self-healing cementitious materials: an all-inclusive overview on progress, benefits and challenges, Sustainability 14 (4) (2022) 1980.
[42] D.Y. Zhu, M.Z. Rong, M.Q. Zhang, Self-healing polymeric materials based on microencapsulated healing agents: from design to preparation, Prog. Polym. Sci. 49 (2015) 175–220.
[43] M. Somasri, B.N. Kumar, Graphene oxide as Nano material in high strength self-compacting concrete, Mater. Today:. Proc. 43 (2021) 2280–2289.
[44] W. Zhang, et al., Self-healing cement concrete composites for resilient infrastructures: A review, Compos. B Eng. 189 (2020), 107892.
[45] H. Kim, et al., Recent advances in microbial viability and self-healing performance in bacterial-based cementitious materials: a review, Constr. Build. Mater. 274 (2021), 122094.
[46] W. Jiang, et al., Synthesis and self-healing properties of composite microcapsule based on sodium alginate/melamine-phenol–formaldehyde resin, Constr. Build. Mater. 271 (2021), 121541.
[47] J. Wang, et al., Application of hydrogel encapsulated carbonate precipitating bacteria for approaching a realistic self-healing in concrete, Constr. Build. Mater. 68 (2014) 110–119.
[48] G. Anglani, et al., Durability of self-healing cementitious systems with encapsulated polyurethane evaluated with a new pre-standard test method, Mater. Struct. 55 (5) (2022) 143.
[49] Guo, S. and S. Chidiac. Self-healing concrete: A critical review. in Proceedings of the, CSCE Annual Conference, Laval, QC, Canada, 2019, p. 2019.
[50] J. Wang, et al., Application of modified-alginate encapsulated carbonate producing bacteria in concrete: a promising strategy for crack self-healing, Front. Microbiol. 6 (2015) 1088.
[51] X. Xiao, et al., Development of a functionally graded bacteria capsule for self-healing concrete, Cem. Concr. Compos. 136 (2023), 104863.
[52] M. Sahmaran, G. Yildirim, T.K. Erdem, Self-healing capability of cementitious composites incorporating different supplementary cementitious materials, Cem. Concr. Compos. 35 (1) (2013) 89–101.
[53] M. Li, and S, Fan, Designing repeatable Self-healing into cementitious materials, 2016.
[54] J.W. Pang, I.P. Bond, A hollow fibre reinforced polymer composite encompassing self-healing and enhanced damage visibility, Compos. Sci. Technol. 65 (11–12) (2005) 1791–1799.
[55] M. Araújo, et al., Poly (methyl methacrylate) capsules as an alternative to the ''proof-of-concept''glass capsules used in self-healing concrete, Cem. Concr. Compos. 89 (2018) 260–271.
[56] V.C. Li, Y.M. Lim, Y.-W. Chan, Feasibility study of a passive smart self-healing cementitious composite, Compos. B Eng. 29 (6) (1998) 819–827.
[57] Khaneghahi, Mohammad Houshmand, Divya Kamireddi, Seyed Ali Rahmaninezhad, Caroline L. Schauer, Christopher M. Sales, Ahmad Najafi, Aidan Cotton, Amir Sadighi, and Yaghoob Amir Farnam. Development of bio-inspired multi-functional polymeric-based fibers (BioFiber) for advanced delivery of bacterial-based self-healing agent in concrete. In *MATEC Web of Conferences*, vol. 378, p. 02001. EDP Sciences, 2023.
[58] D. Bekas, et al., Self-healing materials: a review of advances in materials, evaluation, characterization and monitoring techniques, Compos. B Eng. 87 (2016) 92–119.
[59] Rahmaninezhad, Seyed Ali, Mohammad Houshmand Khaneghahi, Yaghoob Amir Farnam, Caroline L. Schauer, Ahmad Najafi, Reva M. Street, Amir Sadighi, Divya Kamireddi, and Christopher M. Sales. Understanding the importance of endosporulation methods for generating endospores that can resist harsh conditions and produce calcite in bio self-healing of concrete. In *MATEC Web of Conferences*, vol. 378, p. 02004. EDP Sciences, 2023.
[60] Rahmaninezhad, S.A., et al., Influence of culturing media components on the growth and microbial induced calcium carbonate precipitation (MICP) activity of Lysinibacillus sphaericus. bioRxiv, 2022: p. 2022.05. 23.493178.
[61] M.G. Sohail, et al., Bio self-healing concrete using MICP by an indigenous Bacillus cereus strain isolated from Qatari soil, Constr. Build. Mater. 328 (2022), 126943.
[62] J. Intarasoontron, et al., Comparing performances of MICP bacterial vegetative cell and microencapsulated bacterial spore methods on concrete crack healing, Constr. Build. Mater. 302 (2021), 124227.
[63] M. Gao, et al., Immobilized bacteria with pH-response hydrogel for self-healing of concrete, J. Environ. Manage. 261 (2020), 110225.
[64] A. Dsouza, et al., Multifunctional composite hydrogels for bacterial capture, growth/elimination, and sensing applications, ACS Appl. Mater. Interfaces 14 (42) (2022) 47323–47344.
[65] P. Heng, L. Chan, T. Wong, Formation of alginate microspheres produced using emulsification technique, J. Microencapsul. 20 (3) (2003) 401–413.
[66] A. Ching, et al., Impact of cross-linker on alginate matrix integrity and drug release, Int. J. Pharm. 355 (1–2) (2008) 259–268.
[67] H. Ferral-Pérez, et al., Novel method to achieve crystallinity of calcite by Bacillus subtilis in coupled and non-coupled calcium-carbon sources, AMB Express 10 (2020) 1–10.
[68] Scrivener, K., R. Snellings, and B. Lothenbach, A practical guide to microstructural analysis of cementitious materials. Vol. 540. 2016: Crc Press Boca Raton, FL, USA:.